



# Remarkable effect of postsynthesis preparation procedures on catalytic properties of Ni-loaded BEA zeolites in hydrodechlorination of 1,2-dichloroethane

A. Śrębowa<sup>a,\*,\*\*</sup>, R. Baran<sup>b,c,d</sup>, D. Łomot<sup>a</sup>, D. Lisovytskiy<sup>a</sup>, T. Onfroy<sup>b,c</sup>, S. Dzwigaj<sup>b,c,\*</sup>

<sup>a</sup> Institute of Physical Chemistry, PAS, ul. Kasprzaka 44/52, PL-01224 Warszawa, Poland

<sup>b</sup> UPMC Université Paris 06, Laboratoire de Réactivité de Surface, Case 178, Site d'Ivry-Le Raphaël, 3 rue Galilée, 94200 Ivry sur Seine, France

<sup>c</sup> CNRS-UMR 7197, Laboratoire de Réactivité de Surface, Case 178, Site d'Ivry-Le Raphaël, 3 rue Galilée, 94200 Ivry sur Seine, France

<sup>d</sup> AGH University of Science and Technology, al. A. Mickiewicza 30, 30-059 Krakow, Poland

## ARTICLE INFO

### Article history:

Received 31 May 2013

Received in revised form 30 July 2013

Accepted 26 August 2013

Available online 1 September 2013

### Keywords:

Ni

BEA

Hydrodechlorination

1,2-Dichloroethane

## ABSTRACT

$\text{Ni}_{2,0}\text{SiBEA}$  and  $\text{Ni}_{2,0}\text{HAI}BEA$  zeolites were prepared by two different procedures: (i) a two-step postsynthesis method that consist of (1) creation of vacant T-atom sites by dealumination of HAI $\text{BEA}$  ( $\text{Si}/\text{Al} = 17$ ) with nitric acid and then (2) impregnation of as resulting Si $\text{BEA}$  ( $\text{Si}/\text{Al} > 1300$ ) with aqueous nickel nitrate solution and (ii) conventional wet impregnation of HAI $\text{BEA}$  ( $\text{Si}/\text{Al} = 17$ ) respectively. The calcination of  $\text{Ni}_{2,0}\text{SiBEA}$  and  $\text{Ni}_{2,0}\text{HAI}BEA$  at 773 K for 3 h in air led to the formation of C- $\text{Ni}_{2,0}\text{SiBEA}$  and C- $\text{Ni}_{2,0}\text{HAI}BEA$  with appearance, for the former mainly pseudo-tetrahedral Ni(II) incorporated in BEA framework and for the latter, pseudo-tetrahedral and extra-framework octahedral Ni(II) as evidenced by XRD, DR UV-vis and XPS. After reduction at 873 K for 3 h in flowing 10%  $\text{H}_2/\text{Ar}$ , red-C- $\text{Ni}_{2,0}\text{SiBEA}$  and red-C- $\text{Ni}_{2,0}\text{HAI}BEA$  were obtained and investigated as the catalysts in hydrodechlorination of 1,2-dichloroethane at 523–543 K. The activity of the catalysts carried out at atmospheric pressure depended on the reaction temperature, nature of nickel species present in C- $\text{Ni}_{2,0}\text{SiBEA}$  and C- $\text{Ni}_{2,0}\text{HAI}BEA$ , acidity of zeolites, distribution and size of nickel nanoparticles present in red-C- $\text{Ni}_{2,0}\text{SiBEA}$  and red-C- $\text{Ni}_{2,0}\text{HAI}BEA$  catalysts. Selectivity to desired product – ethylene was very high for red-C- $\text{Ni}_{2,0}\text{SiBEA}$  (~90%) and low for red-C- $\text{Ni}_{2,0}\text{HAI}BEA$  (maximally 30%). The latter catalyst promoted strongly formation of vinyl chloride (up to ~70%). We have shown that prepared by two-step postsynthesis procedure red-C- $\text{Ni}_{2,0}\text{SiBEA}$  was more resistant to sintering during hydrodechlorination of 1,2-dichloroethane than red-C- $\text{Ni}_{2,0}\text{HAI}BEA$  prepared by conventional wet impregnation.

© 2013 Elsevier B.V. All rights reserved.

## 1. Introduction

Chlorinated volatile organic compounds (CVOCs) are widely used in industry as solvents and substrates in plastic productions. However their emission into ecosystems causes serious contamination of air, soils and ground water. The common treatment operations of the waste stream containing chlorinated hydrocarbons are catalytic oxidation, biological degradation and photo-catalytic decomposition. Nowadays, it is very important to develop methods allowing not only to remove but also to convert

harmful substances into useful and nontoxic products and reuse them [1,2].

Catalytic hydrodechlorination (HDC) is considered to be one of the most universal resource-saving methods of reprocessing chloroorganic compounds from both an environmental and an economic point of view [3].

1,2-Dichloroethane (DCE) represents chlorinated hydrocarbon and it was tested in HDC reaction many times. According to literature [4–7], DCE may be converted into four main products: ethylene, ethane, vinyl chloride and ethyl chloride depending on the kind of catalyst used. Ethylene and vinyl chloride are the most desirable products from the point of view of industrial application.

The preparation of efficient catalyst of hydrodechlorination with high selectivity into useful compound require obtaining of well dispersed metal species. Very often the catalysts with mixing composition of noble metals such as Pd and Pt and the transition metals such as Cu, Co, Fe, Ag, or Ni [8–13] are used. Although, such prepared catalysts give promising results, this is not a sufficient solution

\* Corresponding author at: UPMC Université Paris 06, Laboratoire de Réactivité de Surface, Case 178, Site d'Ivry-Le Raphaël, 3 rue Galilée, 94200 Ivry sur Seine, France.  
Tel.: +33 1 44 27 2113; fax: +33 1 44 27 21 13.

\*\* Corresponding author. Tel.: +48 22 343 3215.

E-mail addresses: [asrebowa@ichf.edu.pl](mailto:asrebowa@ichf.edu.pl) (A. Śrębowa), [stanislaw.dzwigaj@upmc.fr](mailto:stanislaw.dzwigaj@upmc.fr) (S. Dzwigaj).

because the price of precious metal restrict their commercial application.

Now, efforts are concentrated in the development of a new method to improve the properties of metal loaded catalysts based on the modification of structure composition and acid–base properties of catalyst supports such as alumina, activated carbons, silica and recently zeolites as well as on looking for a new efficient method of metal impregnation allowing control of product selectivity in HDC process [14–17].

As reported earlier [18], it is possible to control the speciation of nickel species in BEA zeolite by using two-step postsynthesis procedure. In the first step of this procedure, vacant T-atom sites could be created by dealumination of BEA zeolite with nitric acid, and then, in the second step, nickel could be incorporated into resulting materials by using aqueous solution of nickel precursor.

The aim of this study is to investigate the effect of the postsynthesis preparation procedure on the properties of Ni-loaded BEA zeolites in catalytic conversion of 1,2-dichloroethane into ethylene and vinyl chloride.  $\text{Ni}_{2.0}\text{SiBEA}$  and  $\text{Ni}_{2.0}\text{HAI}BEA$  zeolites were prepared by two-step postsynthesis procedure and conventional wet impregnation, respectively, and characterized by chemical analysis, X-ray diffraction (XRD), Fourier transformed infrared spectroscopy (FTIR), temperature-programmed reduction (TPR), diffuse reflectance UV-vis spectroscopy (DR UV-vis) and X-ray photoelectron spectroscopy (XPS). To detect species which can be removed by hydrogen from spent catalysts a temperature-programmed hydrogenation (TPH) has been performed. To determine nickel nanoparticles size distribution in reduced and spent catalysts TEM and STEM were used.

## 2. Experimental

### 2.1. Catalysts preparation

A tetraethylammonium BEA (TEABEA) ( $\text{Si}/\text{Al} = 17$ ) zeolite provided by RIPP (China) was calcined in air ( $100\text{ K h}^{-1}$ ) at  $823\text{ K}$  for  $15\text{ h}$  under static condition to remove the organic template. Organic-free BEA zeolite was separated into two portions. The first portion ( $4\text{ g}$ ) was treated with  $400\text{ mL}$  of  $13\text{ mol L}^{-1}$  nitric acid solution ( $353\text{ K}$ ,  $4\text{ h}$ ) to obtain dealuminated SiBEA zeolite ( $\text{Si}/\text{Al} > 1300$ ) that then was washed several times with distilled water and dried at  $363\text{ K}$  overnight.

Second fraction ( $4\text{ g}$ ) of calcined BEA zeolite was treated two times with  $400\text{ mL}$  of  $0.1\text{ mol L}^{-1}$   $\text{NH}_4\text{NO}_3$  solution during  $3\text{ h}$  in order to exchange  $\text{K}^+$  and  $\text{Na}^+$  ions present in industrial BEA zeolite, for  $\text{NH}_4^+$  ion. Then, the solid was washed with distilled water and dried overnight at  $363\text{ K}$ . The  $\text{NH}_4\text{Al}BEA$  sample was calcined in air ( $100\text{ K h}^{-1}$ ) for  $3\text{ h}$  at  $773\text{ K}$  under static condition to remove  $\text{NH}_3$  and obtain acidic form of zeolite BEA, HAI $BEA$ .

$\text{Ni}_{2.0}\text{SiBEA}$  and  $\text{Ni}_{2.0}\text{HAI}BEA$  were prepared by impregnation of  $2\text{ g}$  of SiBEA and HAI $BEA$ , respectively, with  $2.4 \times 10^{-3}\text{ mol L}^{-1}$  aqueous solution of  $\text{Ni}(\text{NO}_3)_2 \cdot 6\text{H}_2\text{O}$ . Firstly, a solid suspension was stirred for  $24\text{ h}$  at  $298\text{ K}$  in excess solvent using  $200\text{ mL}$  of the nickel solution. Then, the suspension was stirred in evaporator under vacuum of a water pump for  $2\text{ h}$  in air at  $333\text{ K}$  until the water was completely evaporated.

$\text{Ni}_{2.0}\text{SiBEA}$  and  $\text{Ni}_{2.0}\text{HAI}BEA$  were further calcined in air ( $100\text{ K h}^{-1}$ ) at  $773\text{ K}$  for  $3\text{ h}$  under static condition and labeled C- $\text{Ni}_{2.0}\text{SiBEA}$  and C- $\text{Ni}_{2.0}\text{HAI}BEA$ , respectively. Then, a portion of C- $\text{Ni}_x\text{SiBEA}$  and C- $\text{Ni}_x\text{HAI}BEA$  were reduced ( $100\text{ K h}^{-1}$ ) at  $873\text{ K}$  for  $3\text{ h}$  in flowing  $10\%$   $\text{H}_2/\text{Ar}$  to obtain red-C- $\text{Ni}_{2.0}\text{SiBEA}$  and red-C- $\text{Ni}_{2.0}\text{HAI}BEA$ , respectively, where C- stands for calcined and red- for reduced. The catalysts after kinetic run were labeled as spent-C- $\text{Ni}_{2.0}\text{SiBEA}$  and spent-red-C- $\text{Ni}_{2.0}\text{HAI}BEA$ , respectively.

### 2.2. Catalyst characterization

Chemical analysis of each studied zeolite material was performed three times at room temperature on SPECTRO X-Lab Pro apparatus. The average values of these three measurements obtained for Al, Si and Ni were used for calculation of Si/Al ratio and Ni wt%.

X-ray diffractograms (XRD) of as prepared samples were recorded at ambient atmosphere on a BRUKER D8 Advance diffractometer using the  $\text{Cu K}_\alpha$  radiation ( $\lambda = 154.05\text{ pm}$ ). They were recorded in the  $2\theta$  range of  $6\text{--}90^\circ$  with steps of  $0.02^\circ$  and a count time of  $1\text{ s}$  for each step. The catalysts after reduction step and after kinetic run were investigated by a Siemens D5000 diffractometer using Ni-filtered  $\text{Cu K}_\alpha$  radiation.

Analysis of the acidic properties of samples was performed by adsorption of pyridine (Py) followed by infrared spectroscopy. Before analysis, the samples were pressed at  $\sim 1\text{ ton cm}^{-2}$  into thin wafers of ca.  $10\text{ mg cm}^{-2}$  and placed inside the IR cell. Before Py adsorption/desorption experiments, the wafers were activated by calcination under static condition at  $723\text{ K}$  for  $3\text{ h}$  in  $\text{O}_2$  ( $1.6 \times 10^4\text{ Pa}$ ) and then outgassing under secondary vacuum at  $573\text{ K}$  ( $10^{-3}\text{ Pa}$ ) for  $1\text{ h}$ . These wafers were contacted at room temperature with gaseous Py ( $133\text{ Pa}$ ) via a separate cell containing liquid Py. The spectra were then recorded following desorption from  $423$  and  $573\text{ K}$  with a Bruker Vector 22 spectrometer (resolution  $2\text{ cm}^{-1}$ ,  $128$  scans). The reported spectra were obtained after subtraction of the spectrum recorded before Py adsorption. The amount of Brønsted and Lewis acidic centers titrated by pyridine was obtained using a molar extinction coefficient value of  $\varepsilon = 1.67\text{ cm } \mu\text{mol}^{-1}$  for the  $\nu_{19b}$  vibrations of protonated pyridine ( $\text{Py-H}^+$ ) at  $\sim 1540\text{ cm}^{-1}$  and of  $\varepsilon = 2.22\text{ cm } \mu\text{mol}^{-1}$  for the  $\nu_{19b}$  vibrations of coordinated pyridine (Py-L) at  $\sim 1455\text{ cm}^{-1}$  [19].

DR UV-vis spectra were recorded at ambient atmosphere on a Cary 5000 Varian spectrometer (DR UV-vis scan rate  $10\text{ nm s}^{-1}$ , data interval  $1\text{ nm}$ ) equipped with a double integrator with polytetrafluoroethylene as reference.

X-ray photoelectron spectroscopy (XPS) measurements were performed with a hemispherical analyzer (PHOBOS 100, SPECS GmbH) using  $\text{Mg K}_\alpha$  ( $1253.6\text{ eV}$ ) radiation. The power of the X-ray source was  $300\text{ W}$ . The area of the sample analyzed was  $\sim 3\text{ mm}^2$ . The powder samples were pressed on an indium foil and mounted on a special holder. Binding energy (BE) for Si and Ni was measured by reference to the O 1s peak at  $532.5\text{ eV}$ , corresponding to the binding energy of oxygen bonded to silicon. Before analysis, the samples were outgassed at room temperature to a pressure of  $10^{-7}\text{ Pa}$ . All spectra were fitted with a Voigt function (a 70/30 composition of Gaussian and Lorentzian functions) in order to determine the number of components under each XPS peak.

Temperature-programmed reduction (TPR) was carried out using the glass-flow system. TPR runs were performed in flowing  $10\%$   $\text{H}_2/\text{Ar}$  ( $25\text{ cm}^3 \text{ min}^{-1}$ ), ramping the temperature at  $10\text{ K min}^{-1}$  and using a Gow-Mac thermal conductivity detector (TCD). Injections of known amounts of hydrogen into the hydrogen–argon flow were provided for calibration (before and after each TPR run).

Chemisorption measurements of  $\text{H}_2$  and CO using a conventional static method were carried out with a Micromeritics ASAP 2020 Chem instrument. Prior to chemisorption measurement  $0.1\text{ g}$  of C- $\text{Ni}_{2.0}\text{HAI}BEA$  and C- $\text{Ni}_{2.0}\text{SiBEA}$  were reduced in flowing  $10\%$   $\text{H}_2/\text{Ar}$  ( $25\text{ cm}^3 \text{ min}^{-1}$ ), ramping the temperature from room to  $873\text{ K}$  ( $10\text{ K min}^{-1}$ ) and kept at  $873\text{ K}$  for  $3\text{ h}$ . Afterwards the catalysts were cooled down to the room temperature and connected with ASAP 2020 instrument. Next, the samples were heated in flowing He at  $383\text{ K}$  for  $30\text{ min}$  with an additional evacuation for  $10\text{ min}$ . At this temperature, the helium flow was switched for the hydrogen flow and the temperature increased ( $10\text{ K min}^{-1}$ ) to  $653\text{ K}$  and the samples were reduced for  $120\text{ min}$ , subsequently outgassed for

30 min, and finally cooled to 343 K with 30 min evacuation. The hydrogen adsorption isotherm was established. After evacuation at 343 K, a second  $H_2$  isotherm was performed. The gas uptake was obtained by extrapolating to zero pressure the linear portion of the isotherm above the saturation pressure. The first hydrogen isotherm provided the sum of the reversibly and irreversibly adsorbed hydrogen while the second isotherm represented only the reversibly adsorbed hydrogen. The amount of chemisorbed hydrogen was given by the difference. After the second isotherm, the same sample was heated in  $H_2$  at 653 K and outgassed at this temperature for 30 min. Then, the  $H_2$  flow were switched for He and the sample was cooled down to the temperature 298 K with additional 10 min evacuation. CO adsorption isotherms were measured at room temperature and were established similarly like in the case of hydrogen adsorption procedure. The metal dispersion ( $D$ , in %), and metal particle size ( $d$ , in nm) were determined from both the  $H_2$  and CO chemisorption data, assuming that  $H/Ni_s$  ratio equals 1 [20,21] and  $CO/Ni$  equals 0.5 at room temperature [22,23].

The reaction of hydrodechlorination of 1,2-dichloroethane (1,2-DCE), HPLC grade, 99.8% pure from Sigma-Aldrich, Germany was carried out at atmospheric pressure, in a glass flow reactor equipped with fritted disk to place a catalyst charge. Prior to reaction, 0.2 g of the catalyst in powder form, after calcination step at 773 K, was reduced like before chemisorption. Afterwards the catalyst was cooled to 523 K and contacted with the reaction mixture ( $H_2 + Ar + 1,2\text{-DCE}$ ) at  $42 \text{ cm}^3 \text{ min}^{-1}$  ( $2.86 \times 10^{-5} \text{ mol s}^{-1}$ ). 1,2-DCE was provided from a saturator kept at 273 K to give the partial pressure of 1,2-DCA of 2.9 kPa. The partial pressure ratio  $p(H_2)/p(1,2\text{-DCE})$  was 1:1. The flows of  $H_2$  and Ar were fixed by using Bronkhorst Hi-Tec mass flow controllers. The contact time were  $\tau = 0.7 \text{ s}$ , and the space velocity  $SV = 0.0035 \text{ (m}^3 \text{ kg}^{-1} \text{ s}^{-1}\text{)}$ . After screening at 523 K for overnight and reaching a steady-state, the temperature of reaction was gradually increased to 543 K, and new experimental points collected. The reaction was followed by gas chromatography, using a HP5890 series II gas chromatograph with FID, a 5% Fluorcol/Carbopack B column (10 ft) from Supelco. The results of GC analysis were elaborated using HP Chemstation. A satisfactory carbon balance (within ~98%) was found for GC analyses.

HRTEM and HAADF STEM investigations were carried out using FEI TITAN Cubed electron microscope operated at an acceleration voltage of 300 keV and equipped with an energy dispersive X-ray (EDX) EDAX spectrometer. The samples were prepared by dispersing in pure alcohol using ultrasonic cleaner and putting a drop of this suspension on carbon films on copper grids and purified with plasma cleaner.

Temperature-programmed hydrogenation (TPH) were carried out by mass spectrometry (MA200, Dycor-Ametek, Pittsburgh) to detect species which can be removed by hydrogen from used catalysts. During the experiments samples after conversion of 1,2-DCE were heated from room temperature to 1073 K in the flow of 10%  $H_2/He$  with monitoring of twelve masses ( $m/z$ ).

### 3. Results and discussion

#### 3.1. X-ray diffraction

The X-ray diffractograms of HAIPEA,  $Ni_{2.0}\text{HAIPEA}$ , SiBEA and  $Ni_{2.0}\text{SiBEA}$  zeolites (Fig. 1) indicate that the samples are well crystallized and correspond to BEA type zeolite structure. Calcination (at 823 K during 15 h) and dealumination with nitric acid did not affect crystallinity and the samples do not show any evidence of extralattice crystalline compound as reported earlier [24,25].

The X-ray diffractogram of the samples after reduction and after HDC reaction (Fig. 1) do not show significant changes in the case

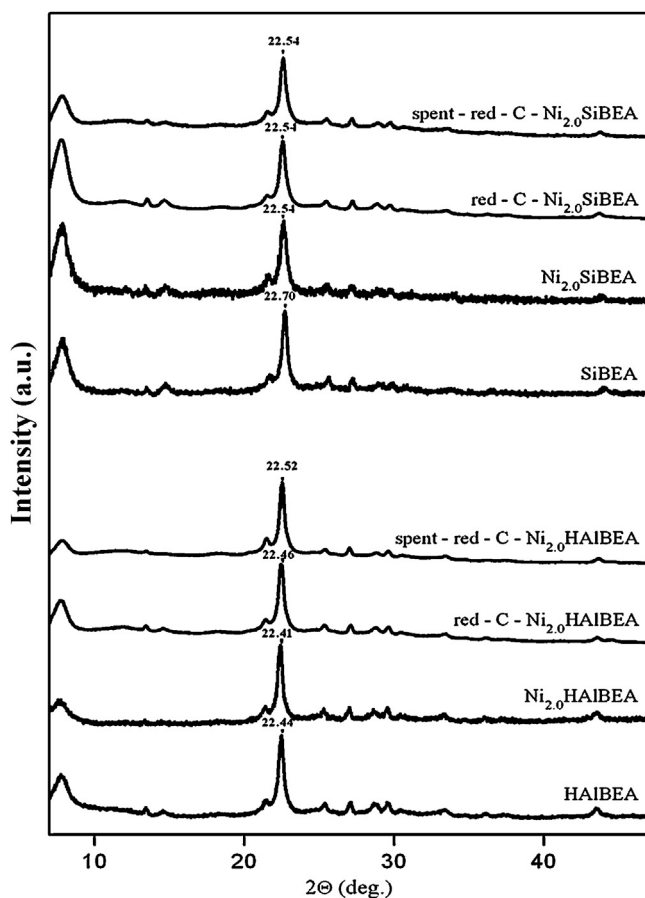


**Fig. 1.** XRD patterns recorded at ambient atmosphere of HAIPEA,  $Ni_{2.0}\text{HAIPEA}$ , red-C- $Ni_{2.0}\text{HAIPEA}$ , spent-red-C- $Ni_{2.0}\text{HAIPEA}$ , SiBEA,  $Ni_{2.0}\text{SiBEA}$ , red-C- $Ni_{2.0}\text{SiBEA}$  and spent-red-C- $Ni_{2.0}\text{SiBEA}$ .

of  $Ni_{2.0}\text{SiBEA}$ . It means that the reduction at 873 K and catalytic process did not cause significant changes of  $Ni_{2.0}\text{SiBEA}$  structure. A little shift of main diffraction peak from  $2\theta = 22.46^\circ$  for red-C- $Ni_{2.0}\text{HAIPEA}$  to  $2\theta = 22.52^\circ$  for spent-red-C- $Ni_{2.0}\text{HAIPEA}$  suggests that hydrodechlorination of 1,2-dichloroethane may cause a little changes in the structure of this zeolite catalyst probably as a result of formation of carbonaceous species and/or irreversible adsorption of HCl in the zeolite, as it has been observed earlier for zeolite materials [26,27].

#### 3.2. FTIR investigation in hydroxyl range and acidity

The FTIR spectrum of activated HAIPEA zeolite exhibits six characteristic bands in OH stretching region: at  $3781$  and  $3660 \text{ cm}^{-1}$  attributed to  $\text{AlO-H}$  groups of extra-framework aluminum species [28,29], at  $3745$  and  $3735 \text{ cm}^{-1}$  associated to isolated external and isolated internal  $\text{SiO-H}$  groups [30], at  $3608 \text{ cm}^{-1}$  related to bridging hydroxyls  $\text{Si-O(H)-Al}$  and at  $3550 \text{ cm}^{-1}$  broad band related to H-bonded  $\text{SiO-H}$  groups.

The introduction of nickel ions into HAIPEA leads to disappearance of broad band at  $3550 \text{ cm}^{-1}$  and narrow band at  $3781 \text{ cm}^{-1}$  (Fig. 2) suggesting that nickel ions interacts with corresponding hydroxyl groups of HAIPEA.

The treatment of organic-free HAIPEA with high concentrated nitric acid solution leads to removal of aluminum atoms and appearance in the spectrum of resulted SiBEA a very intense narrow band at  $3735 \text{ cm}^{-1}$  related to isolated internal  $\text{SiO-H}$  groups (Fig. 2) and an intense broad band at  $3540 \text{ cm}^{-1}$  due to hydrogen bonded silanol groups suggesting formation of vacant T-atom sites,

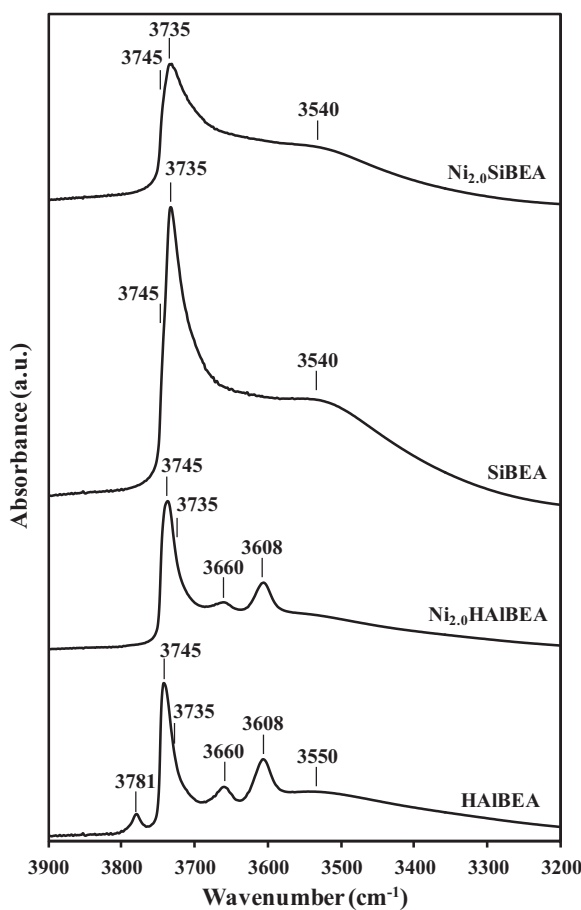


**Fig. 2.** FTIR spectra recorded at room temperature of HAIBEA,  $\text{Ni}_{2.0}\text{HAIBEA}$ , SiBEA and  $\text{Ni}_{2.0}\text{SiBEA}$  in the vibrational range of OH groups.

as reported earlier [31]. The impregnation of SiBEA with aqueous solution of nickel precursor results in strong decreasing of intensity of OH bands of hydrogen bonded silanol groups at  $3540\text{ cm}^{-1}$  (Fig. 2) suggesting that nickel ions react with these silanol groups leading to the incorporation of nickel ions into framework of SiBEA, in line with earlier report [18].

To determine the nature, number and strength of acidic centers of supports and nickel containing samples the FTIR spectra of adsorbed pyridine as probe molecule were recorded.

The FTIR spectra after adsorption of pyridine at room temperature and then outgassed at 423 K are given in Fig. 3. For HAIBEA sample very intense, characteristic bands of pyridinium cations are seen at  $1637$  and  $1546\text{ cm}^{-1}$  suggesting presence of strong Brønsted acidic centers related to proton of  $\text{Si}-\text{O}(\text{H})-\text{Al}$  groups. Furthermore, the band at  $1455\text{ cm}^{-1}$  is related to interaction between pyridine molecules and strong Lewis acidic centers ( $\text{Al}^{3+}$ ) while the band at  $1622\text{ cm}^{-1}$  may be ascribed to pyridine coordinately bonded to Lewis acidic centers [32,33]. Finally, the band at  $1491\text{ cm}^{-1}$  corresponds to C–C oscillation of pyridine aromatic ring chemisorbed on both Brønsted and Lewis acid centers. Additionally, presence of small band at  $1578\text{ cm}^{-1}$  may be associated with pyridine coordinately bonded to weak Lewis acidic centers [34].

Introduction of nickel ions into HAIBEA leads to formation of additional amount of Lewis acidic centers (Fig. 3 and Table 1) confirmed by appearing of intense bands at  $1611$  and  $1449\text{ cm}^{-1}$  and to decrease of quantity of Brønsted acidic centers evidenced by lower intensity of the bands at  $1637$  and  $1546\text{ cm}^{-1}$  for  $\text{Ni}_{2.0}\text{HAIBEA}$  than HAIBEA (Fig. 3). These phenomena may be explained by some

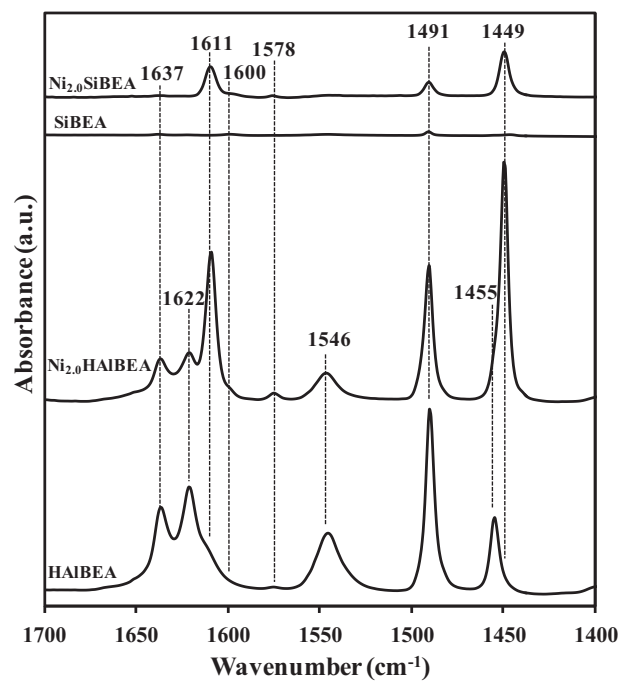


**Fig. 3.** FTIR spectra of HAIBEA,  $\text{Ni}_{2.0}\text{HAIBEA}$ , SiBEA and  $\text{Ni}_{2.0}\text{SiBEA}$  after adsorption of pyridine (133 Pa) for 1 h at room temperature and desorption at 423 K for 1 h.

degree of ion exchange of proton of bridging hydroxyls  $\text{Si}-\text{O}(\text{H})-\text{Al}$  with nickel ions.

As we have recently reported [35], SiBEA contains very small amount of both Brønsted and Lewis acidic centers due to presence of traces of aluminum atoms remaining after nitric acid treatment. The impregnation of SiBEA with the aqueous  $\text{Ni}(\text{NO}_3)_2$  solution leads to increase of amount of Lewis acidic centers evidenced by appearance of FTIR bands at  $1611$  and  $1449\text{ cm}^{-1}$  probably due to pyridine bonded to isolated nickel(II) species.

The results presented in Fig. 3 and Table 1 show that HAIBEA and  $\text{Ni}_{2.0}\text{HAIBEA}$  contain much higher amount of Brønsted and Lewis acidic centers than SiBEA and  $\text{Ni}_{2.0}\text{SiBEA}$ .

### 3.3. Diffuse reflectance UV-vis spectroscopy

DR UV-vis spectra of as-prepared, light green  $\text{Ni}_{2.0}\text{HAIBEA}$  and  $\text{Ni}_{2.0}\text{SiBEA}$  (Fig. 4) look very similar and contain three characteristic bands at  $405$ ,  $665$ – $670$  and  $740\text{ nm}$  [36–38]. All these bands are related to mononuclear  $\text{Ni}(\text{II})$  in octahedral coordination. Two intense bands at  $405$  and  $740\text{ nm}$  are assigned to spin-allowed electron transfer transition  ${}^3\text{A}_{2g}(\text{F}) \rightarrow {}^3\text{T}_{1g}(\text{P})$  and  ${}^3\text{A}_{2g}(\text{F}) \rightarrow {}^3\text{T}_{1g}(\text{F})$ , respectively, and a band at  $665\text{ nm}$  to spin-forbidden one, in line with earlier work [37,39].

For C- $\text{Ni}_{2.0}\text{HAIBEA}$  (calcined at 773 K for 3 h in air), the main absorption bands are located at  $440$ ,  $535$  and  $720$ – $725\text{ nm}$ . The band at  $440$  and  $535\text{ nm}$  are characteristic of ligand–metal charge

**Table 1**

The amounts of the Brønsted and Lewis acidic centers in  $\text{Ni}_{2.0}\text{HAIBEA}$ , HAIBEA,  $\text{Ni}_{2.0}\text{SiBEA}$  and SiBEA.

Sample	Brønsted acidic centers ( $\mu\text{mol g}^{-1}$ ) <sup>a</sup>	Lewis acidic centers ( $\mu\text{mol g}^{-1}$ )
$\text{Ni}_{2.0}\text{HAIBEA}$	138	414
HAIBEA	331	137
$\text{Ni}_{2.0}\text{SiBEA}$	13	83
SiBEA	7	3

<sup>a</sup> Quantification of number of acidic centers in zeolite was done as reported earlier by Emeis [19].

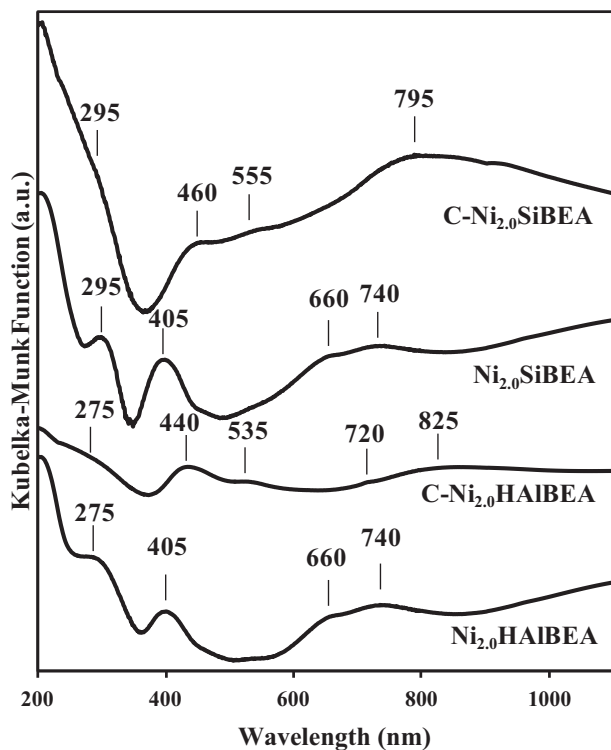


Fig. 4. DR UV-vis spectra recorded at ambient atmosphere of  $\text{Ni}_{2.0}\text{HAIPEA}$ ,  $\text{C-Ni}_{2.0}\text{HAIPEA}$ ,  $\text{Ni}_{2.0}\text{SiBEA}$  and  $\text{C-Ni}_{2.0}\text{SiBEA}$ .

transfer transitions of tetrahedral or distorted tetrahedral (pseudo-tetrahedral) coordinated nickel species [39]. The band at 725 nm may be related to oxygen–octahedral  $\text{Ni}(\text{II})$  charge transfer transition. Thus, it suggests that both pseudo-tetrahedral and octahedral nickel(II) species occur simultaneously in  $\text{C-Ni}_{2.0}\text{HAIPEA}$  zeolites.

For  $\text{C-Ni}_{2.0}\text{SiBEA}$  sample (Fig. 4) the bands present between 450 and 635 nm may be related to  $\text{Ni}(\text{II})$  in tetrahedral or pseudo-tetrahedral coordination and correspond to oxygen–tetrahedral  $\text{Ni}(\text{II})$  charge transfer transition [36,39] indicating that nickel ions are mainly present as pseudo-tetrahedral isolated centers and only few remaining nickel(II) species have octahedral coordination.

### 3.4. Temperature-programmed reduction

Temperature-programmed reduction experiments were carried out to determine the reducibility of nickel ions in  $\text{C-Ni}_{2.0}\text{HAIPEA}$  and  $\text{C-Ni}_{2.0}\text{SiBEA}$ .

The TPR pattern of  $\text{C-Ni}_{2.0}\text{HAIPEA}$  (Fig. 5) contains three peaks present at 645, 770 and 845 K. The observed peaks may be attributed to the reduction of  $\text{Ni}$  ions present in three different states [31]. The signal at 645 K is probably due to reduction of octahedral nickel (II) species present in extra-framework position. The two reduction peaks at 770 and 845 K may be assigned to reduction of two types of tetrahedral  $\text{Ni}(\text{II})$  species strongly interacting with zeolite support. Moreover, for all TPR peaks the reduction temperature is much higher than that observed for  $\text{NiO}$  particles (about 490 K) and reported earlier [40], indicating absence of such kind of nickel species in  $\text{C-Ni}_{2.0}\text{HAIPEA}$ .

The TPR pattern of  $\text{C-Ni}_{2.0}\text{SiBEA}$  (Fig. 5) contains a main peak located at 730 K and two shoulders at 650 and 845 K. Appearance of the main signals at 730 K and 845 K suggests that nickel in  $\text{Ni}_{2.0}\text{SiBEA}$  is well dispersed as two kinds of isolated  $\text{Ni}(\text{II})$  pseudo-tetrahedral species, strongly bound to SiBEA matrix [31,41]. Appearance of reduction peak at 650 K may be explained by the

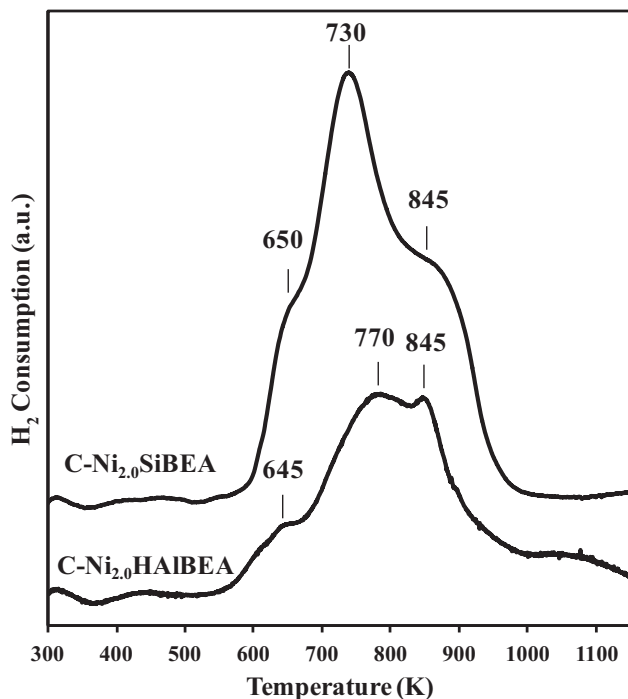


Fig. 5. TPR of  $\text{C-Ni}_{2.0}\text{HAIPEA}$  and  $\text{C-Ni}_{2.0}\text{SiBEA}$ .

presence in  $\text{C-Ni}_{2.0}\text{SiBEA}$  small amount of octahedral  $\text{Ni}(\text{II})$  species, easier reduced to  $\text{Ni}^\circ$  than pseudo-tetrahedral  $\text{Ni}(\text{II})$  one.

The difference between the integral areas of the two TPR curves (Fig. 5) can be due to existence of cationic nickel on the Al-containing sample resisting reduction. In our very last EPR studies, which are under study now, we have observed during  $\text{H}_2$  treatment of NiHAIPEA the formation of both broad signal of  $\text{Ni}^\circ$  nanoparticles and a particular narrow signal with an axial symmetry ( $g_{\parallel} = 2.46$ ;  $g_{\perp} = 2.10$ ) attributed to isolated  $\text{Ni}^+$  species. These EPR signals are also formed upon outgassing of NiHAIPEA at 773 K under vacuum. In contrast, for NiSiBEA  $\text{Ni}^{2+}$  have been very easily reduced to  $\text{Ni}^\circ$  without formation of significant amounts of  $\text{Ni}^+$  even upon outgassing at 773 K under vacuum resulting in creation of very well dispersed  $\text{Ni}^\circ$  nanoparticles. So, it indicates that all Ni are completely reduced to metallic nickel on  $\text{Ni}_{2.0}\text{SiBEA}$  and are only partly reduced to metallic nickel on NiHAIPEA.

The injections of known amounts of hydrogen into the hydrogen–argon flow for calibration (before and after each TPR run) allowed for the calculation of the reducibility of cationic nickel. In contrast to  $\text{C-Ni}_{2.0}\text{SiBEA}$  (100% reducibility), nickel containing HAIPEA showed lower degree of reduction (approximately 90%). It is in agreement with our earlier study for  $\text{Ni}/\gamma\text{-Al}_2\text{O}_3$  [51].

### 3.5. X-ray photoelectron spectroscopy

To elucidate environment and chemical nature of nickel species present in both  $\text{C-Ni}_{2.0}\text{SiBEA}$  and  $\text{C-Ni}_{2.0}\text{HAIPEA}$  zeolites XPS was used.

For  $\text{C-Ni}_{2.0}\text{SiBEA}$  the XP spectrum reveals two signals of  $\text{Ni} 2p_{3/2}$ , first main signal at 856.7 eV attributed to  $\text{Ni}(\text{II})$  species, the most probably to isolated pseudo-tetrahedral  $\text{Ni}(\text{II})$  and second small one at 854.2 eV related to octahedral  $\text{Ni}(\text{II})$  species (Fig. 6), as it has been earlier reported [42,43]. Moreover, in the XPS spectrum of  $\text{C-Ni}_{2.0}\text{SiBEA}$ , in the range of  $\text{Ni} 2p_{1/2}$ , a main signal at 874.7 eV is present, related to framework pseudo-tetrahedral  $\text{Ni}(\text{II})$  formed probably  $\text{Ni}-\text{O}-\text{Si}$  species and also additional peak at 872.3 eV suggesting presence of a little amount of octahedral  $\text{Ni}(\text{II})$ , in line with earlier studies on other nickel containing materials [44–48]. This

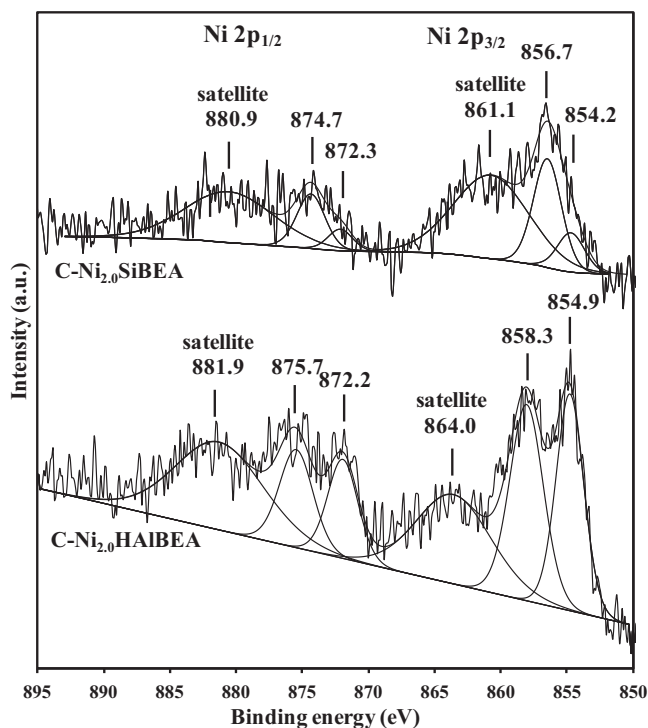


**Fig. 6.** XP spectra recorded at room temperature of Ni 2p core level of C-Ni<sub>2.0</sub>SiBEA and C-Ni<sub>2.0</sub>HAIBEA.

XPS results suggest that nickel in C-Ni<sub>2.0</sub>SiBEA is mainly present as isolated mononuclear pseudo-tetrahedral Ni(II) incorporated into framework of zeolite.

As shown in **Fig. 6**, two peaks of Ni 2p<sub>3/2</sub> occur also in XP spectrum of C-Ni<sub>2.0</sub>HAIBEA catalyst. The peak at BE value of 858.3 eV may be attributed to pseudo-tetrahedral Ni(II), being in strong interaction with the zeolite framework. On the other hand, the peak at 854.9 eV may be attributed to Ni(II) in octahedral coordination. Moreover, in the XPS spectrum of C-Ni<sub>2.0</sub>HAIBEA in the range of Ni 2p<sub>1/2</sub> there are also two main peaks. First at 875.7 eV which may be assigned to pseudo-tetrahedral Ni(II) and second one at 872.2 eV can be attributed to octahedral Ni(II).

Furthermore, it looks like no NiO occurs in both C-Ni<sub>2.0</sub>SiBEA and C-Ni<sub>2.0</sub>HAIBEA which has a distinctively lower binding energy value of  $\sim$ 853 eV. Additionally, the presence of charge transfer satellite peaks of Ni 2p<sub>3/2</sub> at 864.0 eV and Ni 2p<sub>1/2</sub> at 881.9 due to shake-up electrons confirms that nickel occurs in both C-Ni<sub>2.0</sub>SiBEA and C-Ni<sub>2.0</sub>HAIBEA in second oxidation state [45].

The XP spectra of spent-red-C-Ni<sub>2.0</sub>SiBEA was also carried out in the BE region corresponding to Ni 2p and Cl 2p (**Figs. 7 and 8**). The XP spectrum in the BE range of Ni 2p exhibits signal related to one type of nickel species. The values of binding energy of Ni 2p<sub>2/3</sub> at 856.5 eV and of Ni 2p<sub>1/2</sub> at 874.2 eV (**Fig. 7**) as well as of Cl 2p<sub>3/2</sub> at 198.7 eV (**Fig. 8**) indicate that metallic nickel were re-oxidized to Ni(II) species probably due to strong interaction of nickel with chlorine resulting in metal sintering and NiCl<sub>2</sub> formation [49,50] upon long time reaction in agreement with TPH and STEM investigation carried out on spent catalysts (see in the next paragraph). These results strongly confirm poisoning effect of chloride anions on nickel particles and formation of nickel chloride species upon catalytic tests.

### 3.6. Chemisorption results

Chemisorption measurements of H<sub>2</sub> and CO using a conventional static method were effective way to determine dispersion

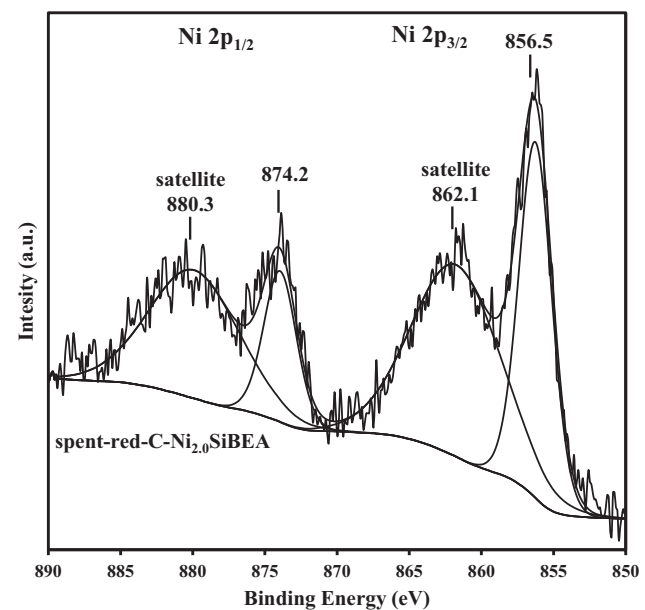


**Fig. 7.** XP spectrum recorded at room temperature of Ni 2p core level of spent-red-C-Ni<sub>2.0</sub>SiBEA.

of nickel in red-C-Ni<sub>2.0</sub>HAIBEA and red-C-Ni<sub>2.0</sub>SiBEA. red-C-Ni<sub>2.0</sub>HAIBEA is characterized by moderate nickel dispersion (20% from H<sub>2</sub> adsorption and 21% from CO adsorption). For red-C-Ni<sub>2.0</sub>SiBEA very high level of nickel dispersion was measured (63% from H<sub>2</sub> adsorption and 66% from CO adsorption). The very high compatibility of the results obtained by H<sub>2</sub> and CO chemisorption was observed which is in accordance with literature [23]. These results are in line with TEM and HAADF STEM investigations (Section 3.8).

### 3.7. Catalytic activity

As it is shown in **Fig. 9**, the red-C-HAIBEA support (Si/Al = 17) exhibits relatively high 1,2-DCE conversion (about 8%), and activity level:  $3.4 \times 10^{-1} \mu\text{mol s}^{-1} \text{g}_{\text{cat}}^{-1}$  at 523 K (after 1000 min of

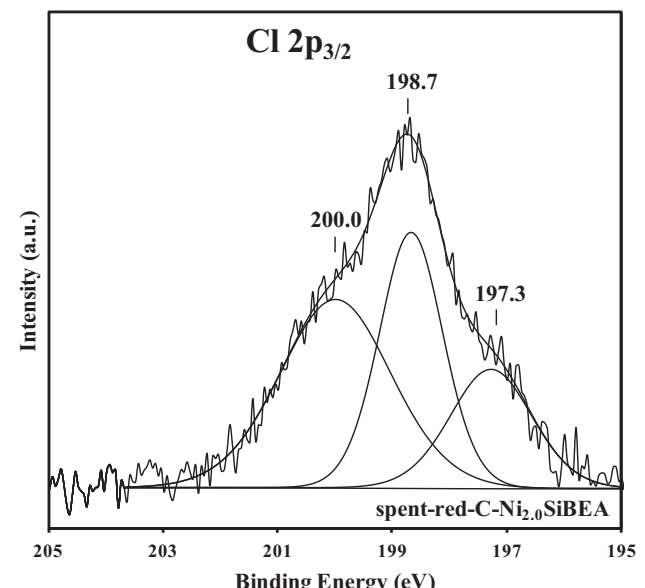


**Fig. 8.** XP spectra recorded at room temperature of Cl 2p core level of spent-red-C-Ni<sub>2.0</sub>SiBEA.

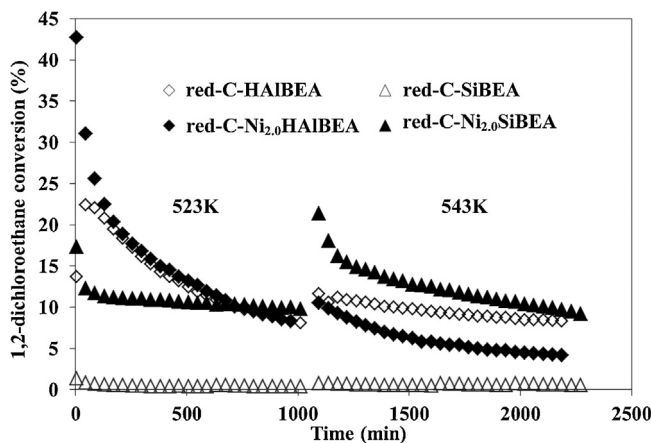


Fig. 9. Time on stream behavior in hydrodechlorination of 1,2-dichloroethane on red-C-HAIBEA, red-C-Ni<sub>2.0</sub>HAIBEA, red-C-SiBEA and red-C-Ni<sub>2.0</sub>SiBEA catalysts at 523 and 543 K: overall conversion.

reaction) and in steady state condition at 543 K, in contrast, red-C-SiBEA support (Si/Al > 1300) exhibits negligible conversion (<0.5%) in both reaction temperatures (Fig. 9). This important difference in catalytic activity of both zeolite supports could be explained by difference in their acidic properties. Indeed, as it is shown in Table 1, HAIBEA support is characterized by much higher concentration of Brønsted and Lewis acidic centers than SiBEA one (7  $\mu\text{mol g}^{-1}$  Brønsted and 3  $\mu\text{mol g}^{-1}$  of Lewis acidic centers for SiBEA and 331  $\mu\text{mol g}^{-1}$  Brønsted and 181  $\mu\text{mol g}^{-1}$  of Lewis acidic centers for HAIBEA). Thus, the presence of Brønsted and Lewis acidic centers seems to play a key role in activity of HAIBEA. Removal of Brønsted and Lewis acidic centers from BEA zeolite upon dealumination leads to SiBEA support almost without acidic centers which could be involved in hydrodechlorination of 1,2-DCE. In spite of the amounts of acidic active centers, both red-C-HAIBEA and red-C-SiBEA showed very low selectivity to ethylene (Fig. 10) and high selectivity (100%) toward vinyl chloride (Fig. 11). It is important to mention here that C<sub>2</sub>H<sub>3</sub>Cl selectivity obtained for red-C-HAIBEA is higher than that observed for  $\gamma$ -Al<sub>2</sub>O<sub>3</sub> in the same conditions [51].

Introduction of nickel ions into HAIBEA support leads to decreasing of the conversion of 1,2-DCE at a steady state condition at 543 K (from 10% for red-C-HAIBEA to ~5% for red-C-Ni<sub>2.0</sub>HAIBEA) (Fig. 9) and reducing activity from  $3.8 \times 10^{-1} \mu\text{mol s}^{-1} \text{g}_{\text{cat}}^{-1}$  to  $1.9 \times 10^{-1} \mu\text{mol s}^{-1} \text{g}_{\text{cat}}^{-1}$ . The reason of this phenomenon may be related to decrease the amounts of Brønsted centers (Table 1 and Fig. 3). Therefore, it seems that two types of acidic centers influence

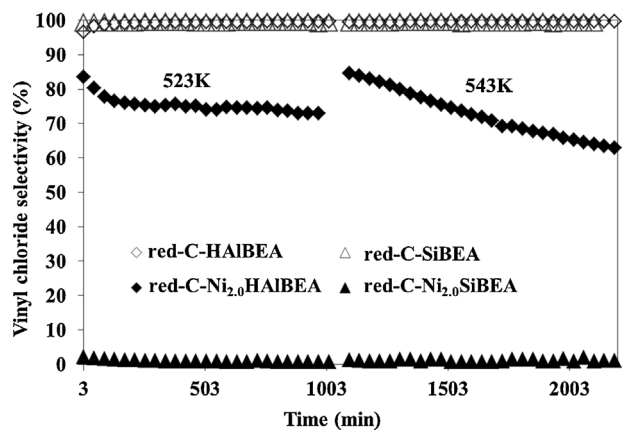


Fig. 11. Time on stream behavior in hydrodechlorination of 1,2-dichloroethane on red-C-HAIBEA, red-C-Ni<sub>2.0</sub>HAIBEA, red-C-SiBEA and red-C-Ni<sub>2.0</sub>SiBEA catalysts at 523 and 543 K: vinyl chloride selectivity.

catalytic behavior of red-C-Ni<sub>2.0</sub>HAIBEA. Catalytic conversion of 1,2-DCE over Brønsted centers leads to formation of vinyl chloride without carbonaceous intermediates. However, conversion of chloroorganic compounds over Ni<sup>2+</sup> Lewis acidic centers can lead to oligomerization of vinyl chloride with intermediate dimer formation of (1,3-dichloro-2-butene), in agreement with earlier report of Shalygin et al. [27]. This is probably the reason of the lower selectivity to vinyl chloride for red-C-Ni<sub>2.0</sub>HAIBEA (~80% at 523 K and above 70% at 543 K) than for red-C-HAIBEA (~100%) (Fig. 11).

In contrast, incorporation of nickel atoms into SiBEA support leads to high increasing of the conversion of 1,2-DCE materials (from less than 0.5% for red-C-SiBEA to higher than 10% for red-C-Ni<sub>2.0</sub>SiBEA) and also significant increasing of activity value from  $1.4 \times 10^{-2} \mu\text{mol s}^{-1} \text{g}_{\text{cat}}^{-1}$  for red-C-SiBEA to  $\sim 3.8 \times 10^{-1} \mu\text{mol s}^{-1} \text{g}_{\text{cat}}^{-1}$  for red-C-Ni<sub>2.0</sub>SiBEA in both reaction conditions (at 523 K after 1000 min of reaction and at steady state condition at 543 K) (Fig. 9). It means that negligible amounts of acidic centers do not influence on catalytic behavior of red-C-Ni<sub>2.0</sub>SiBEA and hydrodechlorination process is realized successfully in the presence of only nickel species with very high (more than 90%) selectivity toward ethylene (Fig. 10).

Besides acidity, nickel dispersion may play the crucial role in activity of the catalysts in hydrodechlorination process and can explain the differences between two types of catalysts. Nickel particles size were determined by CO chemisorption and HRTEM showed ~5 nm of average nickel particles size for red-C-Ni<sub>2.0</sub>HAIBEA and only ~1.5 nm for red-C-Ni<sub>2.0</sub>SiBEA. Fig. 9 shows that higher nickel dispersion observed for red-C-Ni<sub>2.0</sub>SiBEA guarantee rather stable conversion of 1,2-DCE at 523 K and higher conversion at 543 K than appeared for red-C-Ni<sub>2.0</sub>HAIBEA and red-C-HAIBEA.

For red-C-Ni<sub>2.0</sub>HAIBEA with more than three times higher nickel particles size than for red-C-Ni<sub>2.0</sub>SiBEA, significant deactivation at 523 K, the lowest conversion among all the samples at 543 K (Fig. 9) and another products distribution than for red-C-Ni<sub>2.0</sub>SiBEA were observed (Figs. 10 and 11). The vinyl chloride was the major product for nickel containing HAIBEA zeolite (up to ~80% at 523 K, and ~70% at 543 K) but it was lower than C<sub>2</sub>H<sub>3</sub>Cl selectivity observed for red-C-HAIBEA (~100%) (Fig. 10). So, addition of nickel to HAIBEA has an adverse effect on the overall conversion and selectivity to vinyl chloride at the expense of slightly increased selectivity toward environmentally desired product – ethylene (maximally to 30%).

Moreover, the investigations realized in this work show that the nickel nanoparticles present in both red-C-Ni<sub>2.0</sub>SiBEA and red-C-Ni<sub>2.0</sub>HAIBEA catalysts plays very important role in their catalytic activity. As shown by DR UV-vis and XPS in C-Ni<sub>2.0</sub>SiBEA

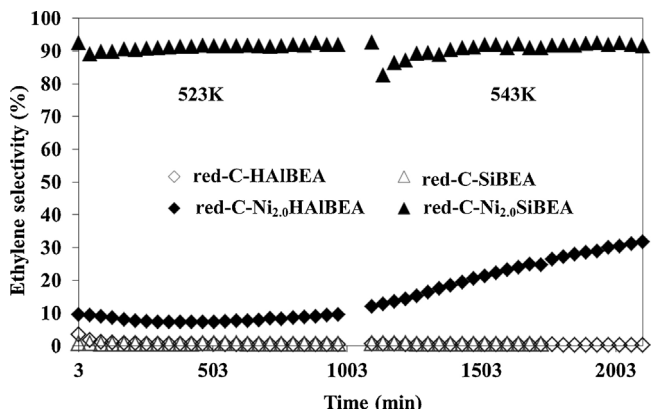
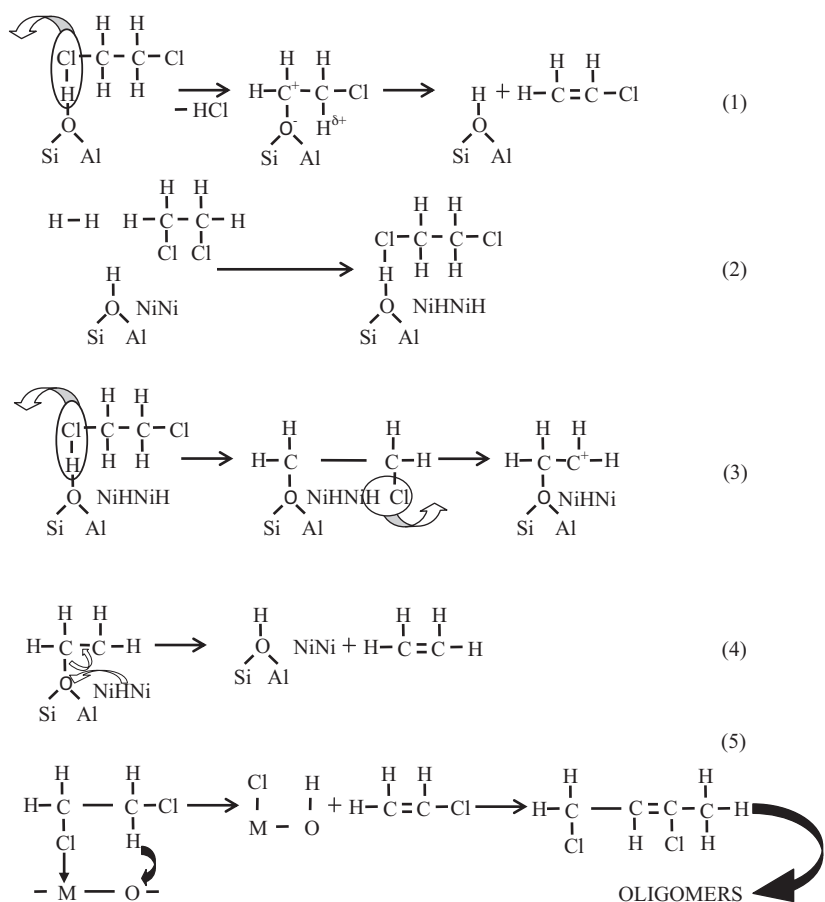


Fig. 10. Time on stream behavior in hydrodechlorination of 1,2-dichloroethane on red-C-HAIBEA, red-C-Ni<sub>2.0</sub>HAIBEA, red-C-SiBEA and red-C-Ni<sub>2.0</sub>SiBEA catalysts at 523 and 543 K: ethylene selectivity.



**Scheme 1.** Proposed probable reaction steps for catalytic conversion of 1,2-dichloroethane over red-C-HAIPEA (1) and red-C-Ni<sub>2.0</sub>HAIPEA (2–5); metallic nickel nanoparticles marked as NiNi, M – coordinatively unsaturated metal atom.

pseudo-tetrahedral Ni(II) are mainly present, in contrast in C-Ni<sub>2.0</sub>HAIPEA additionally octahedral Ni(II) occur. So, the reduction of pseudo-tetrahedral Ni(II) present in C-Ni<sub>2.0</sub>SiBEA leads to formation of excellent dispersed metallic nickel particles active in hydrodechlorination of 1,2-DCE with very high selectivity to ethylene. On the other hand, reduction of the mixture of pseudo-tetrahedral and octahedral Ni(II) present in C-Ni<sub>2.0</sub>HAIPEA (Fig. 6) creates the larger nickel particles than observed after reduction of C-Ni<sub>2.0</sub>SiBEA.

The mechanism of hydrodechlorination of 1,2-DCE on red-C-Ni<sub>2.0</sub>SiBEA was presented earlier [52]. It was suggested that hydrodechlorination toward ethylene takes place on well dispersed metallic nickel particles. The difference in catalytic behavior between red-C-Ni<sub>2.0</sub>SiBEA, red-C-HAIPEA and red-C-Ni<sub>2.0</sub>HAIPEA suggest that the another mechanism of catalytic conversion of 1,2-DCE on the materials with acidic active centers takes place. Inspired by studies of Hannus and Shalygin et al. [26,27], we have proposed a probable mechanism of the catalytic conversion of 1,2-DCE into vinyl chloride and ethylene on red-C-HAIPEA and red-C-Ni<sub>2.0</sub>HAIPEA (Scheme 1). The first step of mechanism (1) shows the typical dehydrochlorination process carried out on acidic centers, where adsorption of 1,2-DCE on Brønsted acidic centers with formation of HCl and vinyl chloride (CH<sub>2</sub>=CHCl) takes place. Simultaneously, Al-O-Si group acquires a hydrogen atom from chloroorganic form, reconstructs the active acidic center and finally vinyl chloride is created as a product of dehydrochlorination of 1,2-DCE on acidic centers of beta zeolite (1). During dehydrochlorination to vinyl chloride on acidic centers may adsorb carbonaceous species [26,27]. And although the presence of hydrogen in reaction mixture does not participate in the mechanism as

the substrate, but it may play a role in removing of carbonaceous species adsorbed on acidic centers and helps with reconstructing them. Addition of nickel to beta zeolite leads to modification of the typical dehydrochlorination mechanism. In the first step of the proposed mechanism (2), dissociative adsorption of hydrogen on nickel centers and the adsorption of 1,2-DCE on acidic centers (from reaction mixture) could occur (2). 1,2-DCE could adsorb on acidic centers through chlorine atom and create vinyl chloride (3). Thanks to hydrogen adsorbed on nickel species it is possible to remove the second Cl atom from adsorbed molecule as HCl (3). Next, desorption of ethylene as the product of reaction and regeneration of acidic centers is observed (4). At lower temperature this reaction leads to formation of mainly vinyl chloride, but at 543 K gradual increasing of ethylene selectivity expense C<sub>2</sub>H<sub>3</sub>Cl is observed. This phenomenon may be the consequence of blockage of acidic centers via strong adsorption of carbonaceous and chlorine containing species. Alternatively, the mechanism of dehydrochlorination may be carried out on Lewis acid-base pair (5). 1,2-DCE is added to metal atom through a chlorine atom, and C–H bond cleaved to OH group. Vinyl chloride is created and it did not desorb from the active centers. It leads to formation of carbonaceous compound and finally oligomers (5) that are probably the cause of red-C-Ni<sub>2.0</sub>HAIPEA deactivation.

Independently on the type of zeolite, deposition of the carbonaceous and chlorine species and the effect of the sintering can influence catalytic behavior of these materials. Extensive research on the causes of catalyst deactivation was led by Heinrichs et al. [53] for Pd–Ag alloys. Based on the results obtained for Pd–Ag alloys we know that deactivation of the catalysts during hydrodechlorination

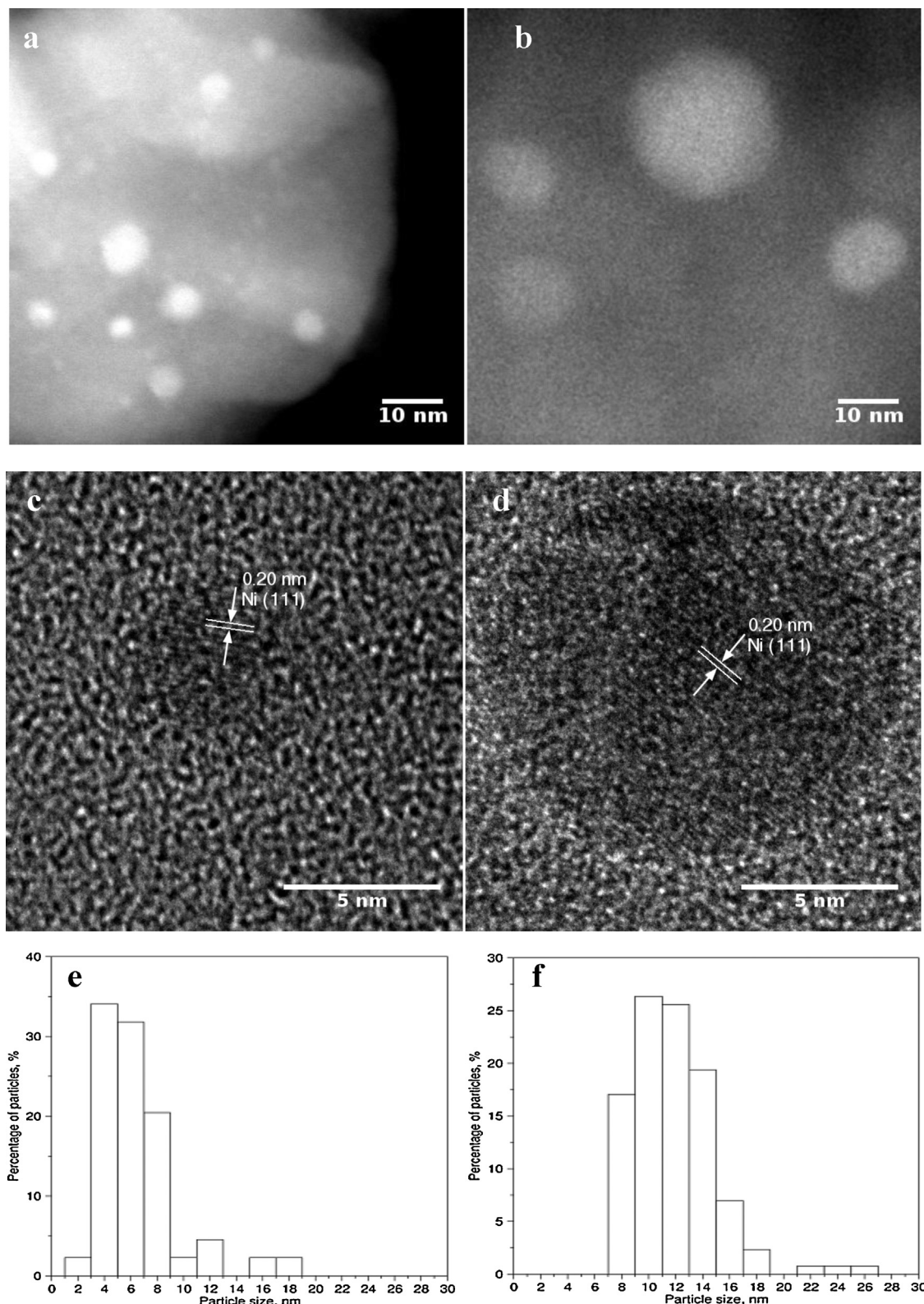


Fig. 12. STEM and HRTEM images and nickel nanoparticle size distribution of red-C-Ni<sub>2.0</sub>HAI BEA (a, c and e) and spent-red-C-Ni<sub>2.0</sub>HAI BEA (b, d and f): effect of sintering.

of 1,2-dichloroethane would be the disappearance of metallic sites (in this case silver sites) either by the gradual formation of stable surface metal chloride or by the deposition of chlorinated carbonaceous residues on those metallic sites, or by both mechanisms. In view of XPS results obtained for spent-catalysts we can adapt this interpretation to deactivation for nickel containing zeolites.

The cause of deactivation of red-C-Ni<sub>2.0</sub>SiBEA and red-C-Ni<sub>2.0</sub>HAI BEA were investigated by TPH of the catalysts after kinetic run and were presented in Section 2.9.

The effect of sintering is not new and is extensively discussed especially for noble metals such as Pd and Pt in hydrodechlorination processes and less often for Ni catalysts [54–58]. It was noted

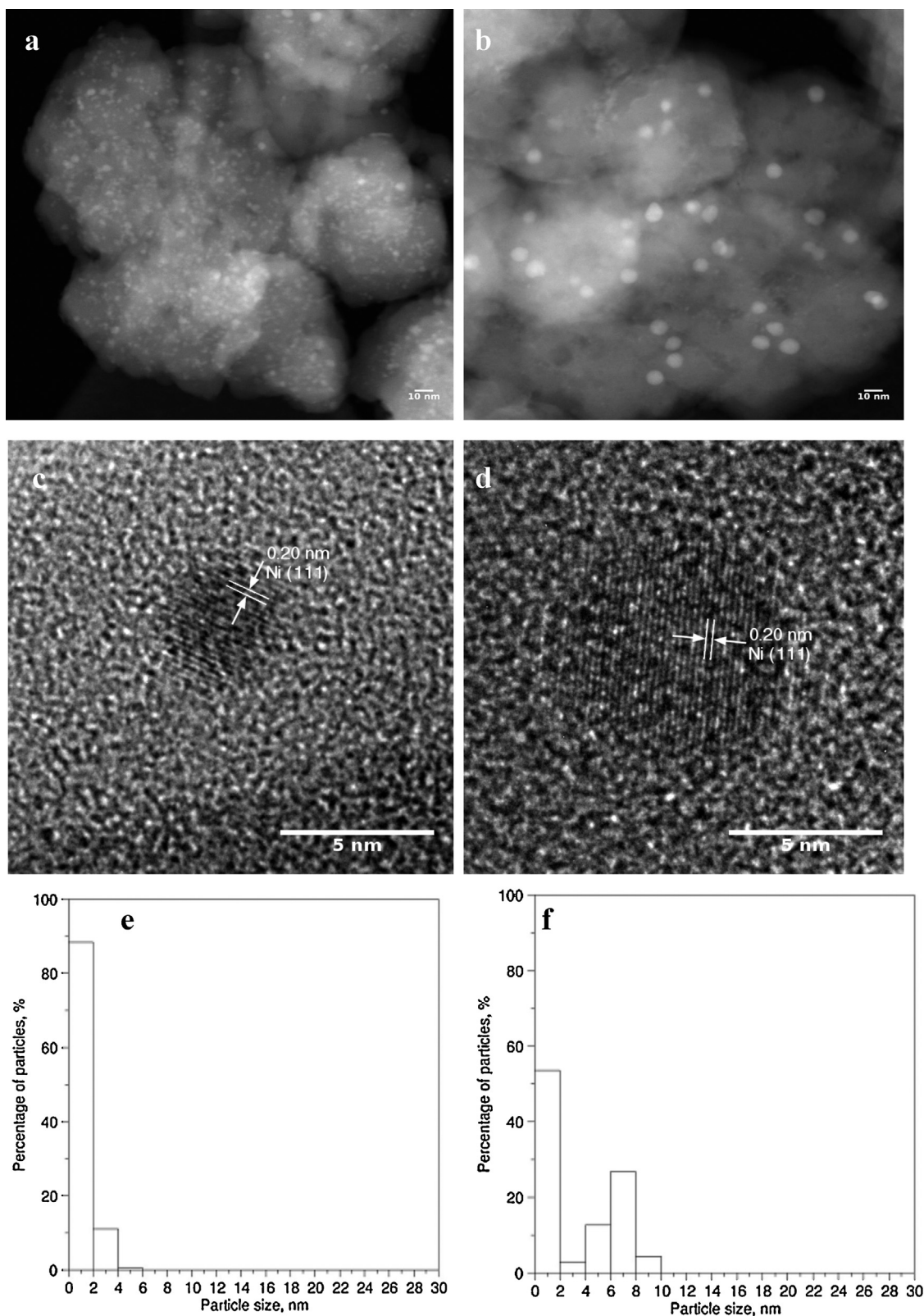


Fig. 13. STEM and HRTEM images and nickel particle size distribution of red-C-Ni<sub>2.0</sub>SiBEA (a, c and e) and spent-red-C-Ni<sub>2.0</sub>SiBEA (b, d and f); effect of sintering.

that sintering of metallic phase depends on various factors. Suh et al. [59] have suggested that the extent of sintering of Pd depends on the properties of the supports. They have shown that the sintering is much more extensive on carbon supports than on Al<sub>2</sub>O<sub>3</sub>. Authors explained this phenomenon by strength of metal–support

interaction in catalysts involving Al<sub>2</sub>O<sub>3</sub> and carbon, so the sintering was much more extensive on carbon support than on Al<sub>2</sub>O<sub>3</sub>. A very strong sintering of carbon supported palladium was already observed during hydrodechlorination of chlorofluorocarbon CFC-115 [60].

As it was shown earlier [61,62], the sintering is responsible for the loss of activity of Ru/C during the gas-phase hydrodechlorination of dichloromethane [61] and platinum supported on alumina and silica during hydrodechlorination of tetrachloromethane, and after the cycle reaction – regeneration [62]. Moon et al. [62] have found that the deactivation of Pd catalysts was caused by the sintering of Pd particles rather than by the cooking. Additionally, they have showed that in the case of hydrodechlorination of chloropentafluoromethane on Pd/Al<sub>2</sub>O<sub>3</sub> and Pd/C, the sintering of metallic phase might be promoted by modification of support or modification of metal phase.

On the other hand Murthy et al. [63] have shown that appreciable Ni particles growth during hydrodechlorination and especially hydrodebromination of 1,3-dichlorobenzene and 1,3-dibromobenzene did not result in any significant loss of catalytic activity of Ni/SiO<sub>2</sub>. The catalyst deactivation was linked to a restructuring of the Ni sites during reaction that serves to disturb hydrogen chemisorption/desorption dynamics.

So, taking into consideration all these literature data we can suppose that the cause of the nickel sintering in red-C-Ni<sub>2.0</sub>SiBEA and red-C-Ni<sub>2.0</sub>HAIPEA is the interaction of the hydrochloride or chlorine, products of hydrodechlorination, with the zeolite. The presence of NiCl<sub>2</sub> detected by XPS for the catalysts after kinetic run suggests that nickel chloride formation plays the key role in nickel sintering for red-C-Ni<sub>x</sub>SiBEA. On the other hand the formation of AgCl in the case of Pd–Ag alloys prevents sintering in the case of small metal particles or even leads to formation of smaller particles size than observed for the fresh metals/support systems [53].

The differences observed in catalytic behavior of red-C-Ni<sub>2.0</sub>SiBEA and red-C-Ni<sub>2.0</sub>HAIPEA catalysts may be related to the initial state of nickel species in mentioned zeolite catalysts. Probably, nickel present in C-Ni<sub>2.0</sub>SiBEA as pseudo-tetrahedral Ni(II) in framework position gives after reduction small and well dispersed nickel nanoparticles which are more resistant to sintering and agglomeration. In contrast, nickel present in C-Ni<sub>2.0</sub>HAIPEA as extra-framework octahedral Ni(II) gives after reduction bigger metal particles less maintained with zeolite structure and more likely to sinter with other nickel particles.

### 3.8. TEM and HAADF STEM results

Fig. 12a–f shows STEM (Fig. 12a and b), HRTEM (Fig. 12c and d) and nickel particles size distributions (Fig. 12e and f) for red-C-Ni<sub>2.0</sub>HAIPEA (Fig. 12a, c and e) and spent-red-C-Ni<sub>2.0</sub>HAIPEA (Fig. 12b, d and f). For red-C-Ni<sub>2.0</sub>HAIPEA the nickel particles are well dispersed in the zeolite structure. An average nickel particle size is ~5 nm in agreement with the results obtained from H<sub>2</sub> and CO chemisorption.

The results obtained for spent-red-C-Ni<sub>2.0</sub>HAIPEA catalysts after kinetic run (Fig. 12 b, d and f) show that the nickel particles are significantly larger than that observed for the catalysts after reduction step.

Fig. 13a–f shows the results obtained for red-C-Ni<sub>2.0</sub>SiBEA and spent-red-C-Ni<sub>2.0</sub>SiBEA. The red-C-Ni<sub>2.0</sub>SiBEA catalyst shows excellent dispersed metal in zeolite material (Fig. 13a, c and e), which was confirmed by presented earlier O<sub>2</sub> chemisorption results [52] and H<sub>2</sub> and CO chemisorption by static method. The nickel particles size distribution for samples before (Fig. 13a, c and e) and after kinetic run (Fig. 13b, d and f) does not show as spectacular changes like in case of red-C-Ni<sub>2.0</sub>HAIPEA. It seems that only the partial increasing of nickel particle size takes place.

TEM and STEM comparison study between C-Ni<sub>2.0</sub>HAIPEA and C-Ni<sub>2.0</sub>SiBEA after reduction at 873 K and after catalytic run may suggest a lower sintering resistance of nickel occurring in red-C-Ni<sub>2.0</sub>HAIPEA zeolite. Furthermore, in view of DR UV–vis, XPS, FTIR

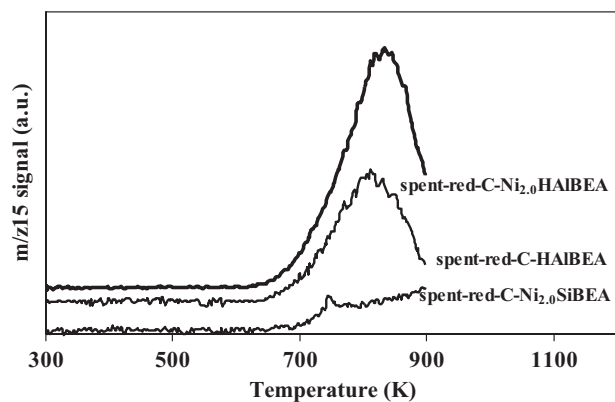


Fig. 14. Temperature-programmed hydrogenation profiles of post-reaction deposition of CH<sub>4</sub> (*m/z* 15) for the catalysts after reaction.

results we can suppose that red-C-Ni<sub>2.0</sub>SiBEA contains mainly very small nickel particles which are more resistant to sintering.

### 3.9. Post-reaction catalysts investigation

Temperature-programmed hydrogenation of post-reaction deposits showed that during catalytic conversion of 1,2-DCE on red-C-Ni<sub>2.0</sub>HAIPEA and red-C-Ni<sub>2.0</sub>SiBEA species containing both carbon and chlorine are deposited. Some accumulation of carbonaceous or/and chlorine species seems important for shaping activity and selectivity of the catalysts, like in case Pd–Ag system where after hydrodechlorination of 1,2-dichloroethane formation of stable silver chloride and/or possibly also the covering of silver sites with chlorinated carbonaceous residues were the cause of deactivation [53]. Significant differences observed for spent-red-C-Ni<sub>2.0</sub>HAIPEA and spent-red-C-Ni<sub>2.0</sub>SiBEA were shown by the representative data obtained for the *m/z* 15 (CH<sub>4</sub>) (Fig. 14), *m/z* 28 (C<sub>2</sub>H<sub>x</sub>) (Fig. 15) and *m/z* 36 (HCl) (Fig. 16) respectively. Comparison study between spent-red-C-HAIPEA and spent-red-C-Ni<sub>2.0</sub>HAIPEA suggests more carbonaceous species on nickel containing zeolite. Some accumulation of C<sub>2</sub>H<sub>4</sub> surface species (*m/z* 28) on spent-red-C-HAIPEA (Fig. 15) confirms the role of acidic centers in process of deactivation of the catalysts. In the case of HCl (*m/z* 36) liberation (Fig. 16) for spent-red-C-Ni<sub>2.0</sub>SiBEA and spent-red-C-Ni<sub>2.0</sub>HAIPEA the same chlorine amount is detected. It means that the same accumulation of chlorine species on both these catalysts during HDC process is strongly related to the presence of metal, in line

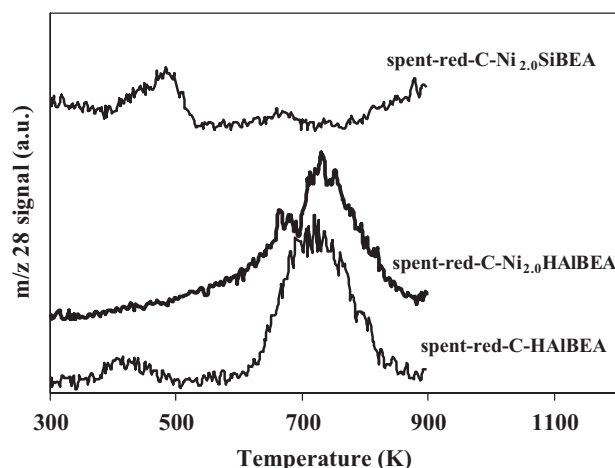
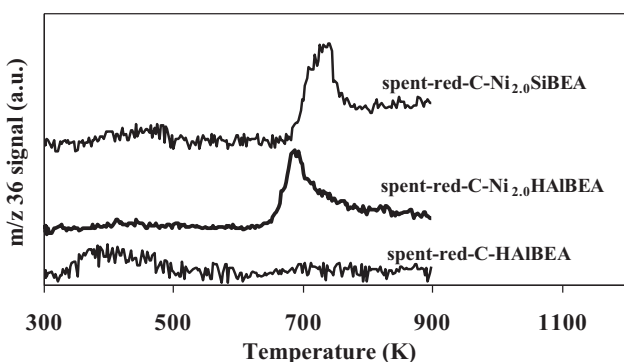


Fig. 15. Temperature-programmed hydrogenation profiles of post-reaction deposition of C<sub>2</sub>H<sub>x</sub> species (*m/z* 28) for the catalysts after reaction.



**Fig. 16.** Temperature-programmed hydrogenation profiles of post-reaction deposition of HCl ( $m/z$  36) for the catalysts after reaction.

with earlier work of Choi and Lee on hydrodechlorination of chloroorganic compounds on typical nickel/support system [64] or for bimetallic Pd–Ag/SiO<sub>2</sub> [53]. The TPH results are in agreement with XPS obtained for the samples after kinetic run (Section 2.5).

#### 4. Conclusions

The investigations realized in this work have shown that catalytic behavior of the nickel containing zeolite materials depends on nature of nickel species incorporated in zeolite, the acidity of the zeolite support and dispersion of nickel particles.

The physicochemical characterization of the catalysts before and after kinetic run have shown that two-step postsynthesis procedure is an effective way for preparation of Ni-containing SiBEA catalysts with an excellent dispersion of nickel nanoparticles.

Red-C-Ni<sub>2.0</sub>SiBEA is the effective catalyst for hydrodechlorination of 1,2-DCE to ethylene (the selectivity higher than 90%).

The conventional wet impregnation procedure, used for preparation of Ni<sub>2.0</sub>HAI BEA, is not a good way for synthesis of the catalyst due to the non-homogeneity of the nickel species. On the other hand, the red-C-Ni<sub>2.0</sub>HAI BEA with acidic centers and larger nickel nanoparticles size is characterized by the lower conversion of 1,2-DCE (>4%), very high selectivity into vinyl chloride (~70%) and high sintering process.

~100% selectivity to C<sub>2</sub>H<sub>3</sub>Cl obtained for red-C-HAI BEA is related to the strong Brønsted acidity of this material.

The deactivation of all catalysts observed during hydrodechlorination of 1,2-DCE can be related to sintering of metallic phase and to carbon and chlorine deposition on active catalytic centers.

As we have shown in this work, red-C-Ni<sub>2.0</sub>SiBEA prepared by two step postsynthesis procedure is more resistant for sintering than red-C-Ni<sub>2.0</sub>HAI BEA prepared by conventional wet impregnation procedure.

#### Acknowledgements

Project funded by the Foundation for Polish Science, POMOST/2011-4/11 co-financed by the EU European Regional Development Fund (AŚ, SD), and operated within International Group of Research (GDRI) “Catalysis for Environment: Depollution, Renewable Energy and Clean Fuels”. Special thanks for Izabela Irena Kamińska from IPC PAS in Warsaw for chemisorption measurements.

#### References

- [1] S. Giacomazzi, N. Cochet, Chemosphere 56 (2004) 1021–1032.
- [2] E.D. Goldberg, Sci. Total Environ. 100 (1991) 17–28.
- [3] V.I. Simagina, O.V. Netskina, E.S. Tayban, O.V. Komova, E.D. Grayfer, A.V. Ischenko, E.M. Pazhetnov, Appl. Catal. A 379 (2010) 87–94.
- [4] S.L. Pirard, J.-P. Pirard, G. Heyen, J.-P. Schoobrechts, B. Heinrichs, Chem. Eng. J. 173 (2011) 801–812.
- [5] N. Job, B. Heinrichs, F. Ferauche, F. Noville, J. Marien, J.-P. Pirard, Catal. Today 102 (2005) 234–241.
- [6] A. Śrębowa, W. Lisowski, J.W. Sobczak, Z. Karpinski, Catal. Today 175 (2011) 576–584.
- [7] A. Lopez-Gaona, J.A. De los Reyes, J. Aguilar, N. Martin, React. Kinet. Mech. Catal. 99 (2010) 177–182.
- [8] S. Lambert, F. Ferauche, A. Brasseur, J.-P. Pirard, B. Heinrichs, Catal. Today 100 (2005) 283–289.
- [9] K.V.R. Chary, P.V.R. Rao, V.V. Rao, Catal. Commun. 9 (2008) 886–893.
- [10] M. Lu, J. Sun, D. Zhang, M. Li, J. Zhu, Y. Shan, React. Kinet. Mech. Catal. 100 (2010) 99–103.
- [11] J. Halász, S. Mészáros, I. Hannus, React. Kinet. Catal. Lett. 87 (2006) 359–365.
- [12] T. Zhoua, Y. Li, T.-T. Lim, Sep. Purif. Technol. 76 (2010) 206–214.
- [13] R.F. Howe, Appl. Catal. A 271 (2004) 3–11.
- [14] J.-T. Feng, Y.-J. Lin, D.G. Evans, X. Duan, D.-Q. Li, J. Catal. 266 (2009) 351–358.
- [15] J. Chen, Y. Chen, Q. Yang, K. Li, C. Yao, Catal. Commun. 11 (2010) 571–575.
- [16] L. Calvo, M.A. Gilarranz, J.A. Casas, A.F. Mohedano, J.J. Rodriguez, Chem. Eng. J. 163 (2010) 212–218.
- [17] E. Finocchio, C. Pistarino, S. Dellepiane, B. Serra, S. Braggio, M. Baldi, G. Busca, Catal. Today 75 (2002) 263–267.
- [18] A. Penkova, S. Dzwigaj, R. Kefirov, K. Hadjiivanov, M. Che, J. Phys. Chem. C 111 (2007) 8623–8631.
- [19] C.A. Emeis, J. Catal. 141 (1993) 347–354.
- [20] M.C.J. Bradford, M.A. Vannice, Appl. Catal. A 142 (1996) 73–96.
- [21] C.H. Bartholomew, R.B. Pannell, J. Catal. 65 (1980) 390–401.
- [22] J.T. Stuckless, N. Al-Sarraf, C.E. Wartnaby, D.A. King, J. Chem. Phys. 99 (1993) 2202–2212.
- [23] L. Znak, J. Zieliński, Appl. Catal. A 413–414 (2012) 132–139.
- [24] R. Hajjar, Y. Millot, P.P. Mansiani, M. Che, S. Dzwigaj, J. Phys. Chem. C 112 (2008) 20167–20175.
- [25] S. Dzwigaj, L. Stievano, F.E. Wagner, M. Che, J. Phys. Chem. Solids 68 (2007) 1885–1891.
- [26] I. Hannus, Appl. Catal. A 189 (1999) 263–276.
- [27] A.S. Shalygin, L.V. Malyshheva, E.A. Paukshtis, Kinet. Catal. 52 (2011) 305–315.
- [28] E. Bourgeat-Lami, F. Fajula, D. Angerat, T. des Courieres, Microporous Mater. 12 (1993) 237–245.
- [29] A. Janin, M. Maache, J.C. Lavalle, J.F. Joly, F. Raatz, N. Szydłowski, Zeolites 11 (1991) 391–396.
- [30] S. Dzwigaj, P. Massiani, A. Davidson, M. Che, J. Mol. Catal. A 155 (2000) 169–182.
- [31] R. Baran, Y. Millot, T. Onfroy, F. Averseng, J.-M. Krafft, S. Dzwigaj, Microporous Mesoporous Mater. 161 (2012) 179–186.
- [32] M. Trejda, M. Ziolek, Y. Millot, K. Chalupka, M. Che, S. Dzwigaj, J. Catal. 281 (2011) 169–176.
- [33] G.M. Robb, W. Zhang, P.G. Smirniotis, Microporous Mesoporous Mater. 20 (1998) 307–316.
- [34] S. Dzwigaj, M. Matsuoka, M. Anpo, M. Che, Microporous Mesoporous Mater. 93 (2006) 248–253.
- [35] R. Baran, Y. Millot, T. Onfroy, J.-M. Krafft, S. Dzwigaj, Microporous Mesoporous Mater. 163 (2012) 122–130.
- [36] L. Espinosa-Alonso, K.P. de Jong, B.M. Weckhuysen, J. Phys. Chem. C 112 (2008) 7201–7209.
- [37] C. Lepetit, M. Che, J. Phys. Chem. 100 (1996) 3137–3143.
- [38] M.A. Zanjanchi, A. Ebrahimian, Mater. Chem. Phys. 110 (2008) 228–233.
- [39] A. Kukovecz, Z. Konya, D. Monter, W. Reschitilowski, I. Kiricsi, J. Mol. Struct. 563–564 (2001) 403–407.
- [40] J. Dedecek, L. Capek, D. Kaucky, Z. Sobalik, B. Wichterlova, J. Catal. 211 (2002) 198–207.
- [41] C.D. Wagner, J. Vac. Sci. Technol. 15 (1978) 518–523.
- [42] Y. Matsumura, K. Tanaka, N. Tode, T. Yazawa, M. Haruta, J. Mol. Catal. A 152 (2000) 157–165.
- [43] T. Lehmann, T. Wolff, C. Hamel, P. Veit, B. Garke, A. Seidel-Morgenstern, Microporous Mesoporous Mater. 151 (2012) 113–117.
- [44] S. Bendezú, R. Cida, J.L.G. Fierro, A. López Agudo, Appl. Catal. A 197 (2000) 47–60.
- [45] H. Kim, K. Kang, H. Kwak, J.H. Kim, Chem. Eng. J. 168 (2011) 775–783.
- [46] G.M. Poncelet, A. Centeno, R. Molina, Appl. Catal. A 288 (2005) 232–242.
- [47] S.R. Kirumakki, B.G. Shpeizer, G.V. Sagar, K.V.R. Chary, A. Clearfield, J. Catal. 242 (2006) 319–331.
- [48] M. Wu, L. Chou, H. Song, Catal. Lett. 142 (2012) 627–636.
- [49] W. Fua, H. Yang, L. Chang, M. Li, H. Bala, Q. Yu, G. Zou, Colloids Surf. A: Physicochem. Eng. Aspects 262 (2005) 71–80.
- [50] J.C. Klein, D.M. Hercules, J. Catal. 82 (1983) 424–436.
- [51] W. Juszczysz, J.C. Colmenares, A. Śrębowa, Z. Karpinski, Catal. Today 169 (2011) 186–191.
- [52] R. Baran, I.I. Kaminska, A. Śrębowa, S. Dzwigaj, Microporous Mesoporous Mater. 169 (2013) 120–127.
- [53] B. Heinrichs, F. Noville, J.-P. Schoobrechts, J.-P. Pirard, J. Catal. 220 (2003) 215–225.
- [54] S. Contarini, S.P. Howletta, C. Rizzo, B.A. De Angelis, Appl. Surf. Sci. 51 (1991) 177–183.
- [55] R. Mariscal, R.M. Navarro, B. Pawelec, J.L.G. Fierro, Microporous Mesoporous Mater. 34 (2000) 181–194.
- [56] C.A. Tolman, W.M. Riggs, W.J. Linn, C.M. King, R.C. Wendt, Inorg. Chem. 12 (1973) 2770–2778.

- [57] J.A. Cecilia, I. Jimenez-Morales, A. Infantes-Molina, E. Rodriguez-Castellon, A. Jimenez-Lopez, *J. Mol. Catal. A* 368–369 (2013) 78–87.
- [58] M. Martino, R. Rosal, H. Sastre, F.V. Diez, *Appl. Catal. B* 20 (1999) 301–307.
- [59] D.J. Suh, T.J. Park, S.K. Ihm, *J. Catal.* 149 (1994) 486–488.
- [60] X. Zheng, Q. Xiao, Y. Zhang, X. Zhang, Y. Zhong, W. Zhu, *Catal. Today* 175 (2011) 615–618.
- [61] M.A. Álvarez-Montero, L.M. Gómez-Sainero, J. Juan-Juan, A. Linares-Solano, J.J. Rodriguez, *Chem. Eng. J.* 162 (2010) 599–608.
- [62] D.J. Moon, M.J. Chun, K.Y. Park, S.I. Hong, *Appl. Catal. A* 168 (1998) 159–170.
- [63] K.V. Murthy, P.M. Patterson, G. Jacobs, B.H. Davis, M.A. Kean, *J. Catal.* 223 (2004) 74–85.
- [64] Y.H. Choi, W.Y. Lee, *Catal. Lett.* 67 (2000) 155–160.